Tribology Transactions

ISSN: 1040-2004 (Print) 1547-397X (Online) Journal homepage: https://www.tandfonline.com/loi/utrb20

Microstructural Alterations in Bearing Steels under Rolling Contact Fatigue: Part 2—Diffusion-Based Modeling Approach

Anurag Warhadpande , Farshid Sadeghi & Ryan D. Evans

To cite this article: Anurag Warhadpande , Farshid Sadeghi & Ryan D. Evans (2014) Microstructural Alterations in Bearing Steels under Rolling Contact Fatigue: Part 2—Diffusion-Based Modeling Approach, Tribology Transactions, 57:1, 66-76, DOI: 10.1080/10402004.2013.847999

To link to this article: https://doi.org/10.1080/10402004.2013.847999

Accepted author version posted online: 02 Oct 2013.
Published online: 26 Dec 2013.

Tribology Transactions, 57: 66-76, 2014

ISSN: 1040-2004 print / 1547-397X online
DOI: 10.1080/10402004.2013.847999

STLE
Society of Tribologists and Lubrication Engineers

Microstructural Alterations in Bearing Steels under Rolling Contact Fatigue: Part 2—Diffusion-Based Modeling Approach

ANURAG WARHADPANDE,[1] FARSHID SADEGHI,[1] and RYAN D. EVANS[2]
[1]School of Mechanical Engineering
Purdue University
West Lafayette
Indiana 47907
[2]Timken Technology Center
Canton, Ohio 44706

The microstructure of rolling element bearings can experience significant transformation when subjected to repetitive contact cycling. In Part 1 of this article, a detailed overview of the known microstructure alteration phenomena was presented and the different mechanisms for describing them proposed by various investigators were critically reviewed. It is agreed generally that the primary path of these structural changes is the decay of martensite due to carbon diffusion, leading to the formation of ferrite and lenticular carbides. Furthermore, these altered regions in the material microstructure can be stress concentration regions leading to crack initiation and propagation. In this article, a J2-based elastic–plastic Voronoi finite element model (previously developed by the authors) is coupled with a carbon diffusion–based model. Using Fick's law for stress-assisted diffusion, the dispersion of carbon in the bearing microstructure is evaluated. A backward Euler finite difference scheme is employed to solve the partial differential equations. The model can accurately predict the onset of martensitic decay and formation of the white etching bands along with their distinctive orientation. A comparison of the numerical results shows good corroboration with experimental observations.

KEY WORDS

Microstructural Alteration; White Etching Bands; Carbon Diffusion; Fick's Law

INTRODUCTION

It is well recognized that significant microstructural changes can occur in bearing steel due to cyclic stressing while in service. Jones *(1)* first reported these changes when he observed a troostite-type structure along with grey lines embedded within this region below the bearing raceway. Figure 1 illustrates a sample micrograph of the altered bearing microstructure. Due to the preferential etching properties of this altered microstructure and their appearance under an optical microscope, the different phases observed in fatigued bearings are known as dark and white etching regions. Another phase called lenticular carbides sandwiches the white etching region, as illustrated in Fig. 2. The most interesting aspect of these structural alterations is the remarkable and repeatable orientation of the white etching bands, as illustrated in Fig. 1. Based on their orientation, the white etching bands are classified into two categories: (1) 30° bands and (2) 80° bands. Lund *(2)* first reported this differentiation. Part 1 (Warhadpande, et al. *(3)*) of this article presents a comprehensive review on the topic of microstructural alterations, which have been a subject of much debate and discussion over the last half century. The primary cause for the appearance of different phases in material microstructure is the decay of parent martensite due to contact cycling. As the martensite structure breaks down, a dark etching region appears, consisting of a defective ferritic phase with homogenously distributed excess carbon mixed with residual martensite. After further contact cycling, white etching regions start developing in the material microstructure. First the 30° bands, which are about 2 μm thick, appear and later the 80° bands, which can grow to 10 μm in thickness, appear above the 30° bands. These white bands are disc-shaped regions of ferrite typically having nanosized grains (Bhadeshia *(4)*).

Over the past few decades, different researchers have presented diverse theories for the marked orientation of the white etching bands (i.e., disc-shaped regions of nanograined ferrite in three dimensions). However, none of the theories satisfactorily explains the formation mechanism of the white etching bands. In order to predict the orientation of the white etching bands, first it is essential to understand the mechanism behind the formation of these bands. Bush, et al. *(5)* postulated an intrusion–extrusion mechanism wherein material intrudes from the regions of carbide particles into the surrounding matrix, which in turn leads to a carbide extrusion in the matrix, thus forming the white etching bands. Martin, et al. *(6)* hinted that there is a link between the plastic deformation of the material due to cyclic reversed plastic

Manuscript received February 17, 2013
Manuscript accepted September 16, 2013
Review led by Daniel Nelias

NOMENCLATURE

A = Proportionality constant
c = Carbon concentration
D = Coefficient of diffusion
E = Young's modulus
J = Diffusion flux
k = Boltzmann's constant
L = Fatigue life
M = Hardening modulus
N = Cycle number
Q = Activation energy
R = Gas constant
r = Radius
T = Temperature
t = Time
V = Potential driving the diffusion process
W_p = Dissipated plastic energy
ε_{ij} = Strain tensor
ν = Poisson's ratio
σ_{ij} = Stress tensor
σ_y = Yield stress

strain in the areas of maximum shear stress that leads to the development of these white bands beneath the surface of a bearing raceway. Buchwald and Heckel *(7)* were the first to provide a detailed materials science–based explanation for the formation of the white etching bands. They proposed that because these bands are different phases developing the material microstructure, the most probable cause for their occurrence is recrystallization. In addition, because any recrystallization process involves the phenomenon of diffusion, carbon diffuses out of the martensite matrix, leading to the formation of regions of low carbon concentration or ferritic discs, which are nothing but the white etching bands. The carbon that diffuses out of the martensite becomes trapped at dislocations or defects or precipitates as layers of cementite/lenticular carbides and hence the white etching bands are found to be sandwiched between the carbon-rich regions of lenticular carbides. Lund *(2)*, who supported this theory, indicated that diffusion is the main source of structural alterations in fatigued bearings. Osterlund and Vingsbo *(8)* and Lindahl and Osterlund *(9)* also supported the idea of diffusion.

Previous investigators have demonstrated that martensite–ferrite phase transformation will determine the structural composition of bearing steel during rolling contact cycling. In 1939, Avrami *(10)–(12)* presented the kinetics of phase transformation in a three-part paper. Based on the Avrami-type equation, researchers developed different models to predict phase transformation with various complexities. Most of these models are based on material-dependent coefficients that are determined by fitting to the experimental results through more advanced

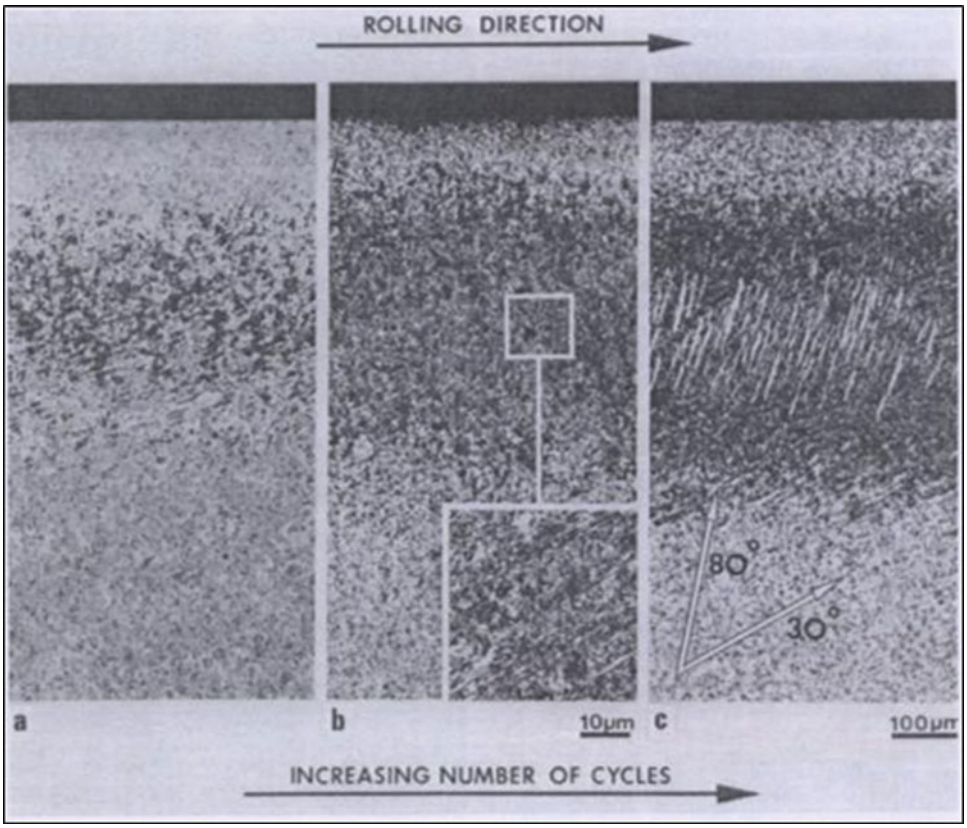

Fig. 1—Microstructural alterations with contact cycling (Swahn, et al. *(24)*) (color figure available online).

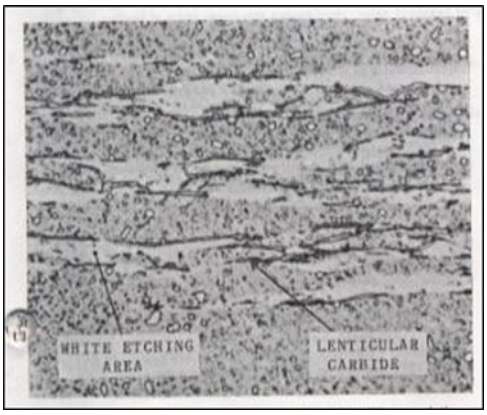

Fig. 2—Optical micrograph of axial section of bearing raceway showing white etching regions and lenticular carbides (Martin, et al. *(6)*) (color figure available online).

phenomenological models (Christian *(13)*; Suehiro, et al. *(14)*; Ronda and Oliver *(15)*) and models based on thermodynamic laws. Pernach and Pietrzyk *(16)* applied a diffusion-based model for modeling austenite–ferrite phase transformation. In this approach, they employed a finite difference method as well as a finite element (FE) method to solve Fick's second law of diffusion. This investigation aimed to determine the influence of physical assumptions and ferrite and austenite grain shape on the kinetics of phase transformation, ferrite volume fraction, ferrite grain size, and carbon segregation. However, in this analysis, preexisting carbon concentration gradients governed the diffusion process. Recently, Zhao *(17)* employed the stress-assisted diffusion equation for modeling oxygen diffusion along grain boundaries in nickel-based superalloy. The diffusion of oxygen was controlled by a gradient of hydrostatic stress in terms of the pressure factor. The present article employs a similar stress-assisted diffusion law (which is an extension of Fick's second law with additional source terms) to model the diffusion of carbon within the near-surface regions of bearing steel during rolling contact fatigue. The study assumes that dissipated plastic energy during elastic–plastic loading is the primary driver of carbon diffusion. To this end, it utilizes the elastic–plastic model developed by Warhadpande, et al. *(18)* to determine the dissipated energy in each cycle. Next, this article solves the stress-assisted diffusion equation using a finite difference scheme, determining the resultant changes in carbon concentration. It is observed that carbon migration occurs along specific directions in the material domain that resemble the orientation of white etching bands. Thus, by using the carbon diffusion–based model in conjunction with the elastic–plastic model, the development of white etching bands during rolling contact fatigue can be simulated.

FICK'S LAWS OF DIFFUSION

Many metallurgists are interested in changes in structural properties of materials and their dependence on physical and mechanical properties. Because many structural changes occur by diffusion, fundamental understanding of phase changes, homogenization, spheroidization, etc., require detailed knowledge of diffusion processes and driving forces. The kinetic process of phase change is treated herein by assuming that the material is a continuum; that is, by ignoring the atomic structure of the solid. With this assumption, the problem reduces to obtaining and solving appropriate differential equations. Fick developed well-known constitutive laws for the diffusion phenomenon. As a simple illustrative example, consider two chambers, one filled with Cu atoms and other with Ni, as illustrated in Fig. 3, separated by a thin membrane.

If the membrane is removed, the atoms in both of the chambers will begin to diffuse into the neighboring chamber because of the concentration gradient. The process will continue as long as the concentration gradient exists. The bidirectional atom flux across the membrane for the diffusion process is directly proportional to the concentration gradient, which is given by Fick's first law.

$$J = -D\left[\frac{\partial c}{\partial x}\right], \qquad [1]$$

where D is the diffusion coefficient. This equation implies that the flux goes to zero as the concentration becomes completely homogenous. However, the above equation does not provide any insight about the concentration of each species as a function of time. The temporal information of change in concentration is provided by Fick's second law, given by

$$\frac{\partial c}{\partial t} = D\nabla^2 c, \qquad [2]$$

where $\nabla^2 c$ is the Laplacian of c. The above equation can be employed in order to determine the concentration at any given instance of time. Because the diffusion occurs due to the presence of a preexisting concentration gradient, this process is termed *self-diffusion*. Figure 3 depicts the change in the concentration after certain time t. From this figure, it is clear that, over time, the diffusion process works to homogenize the mixture.

The above two laws can be employed to determine the concentration of a diffusing media under the presence of a preexisting concentration gradient. However, if the diffusion process is influenced by an external source term, the first and second laws of diffusion require modification. Under such scenarios, an external potential gradient drives the atomic flux, and this flux must be added to that produced by the preexisting concentration gradient in order to arrive at the equation for the total flux. An example of such a diffusion process is stress-assisted diffusion. Shewmon *(18)* provides the equation for the flux under a stress-assisted diffusion scenario:

$$J = -D\left(\nabla c + \frac{c\nabla V}{kT}\right), \qquad [3]$$

where V is the potential driving the diffusion process; k is the Boltzmann constant, 1.38×10^{-23} J/K; and T is the temperature (in Kelvin). The current analysis assumes isothermal conditions with $T = 373$ K. Using this equation for flux, the equation for concentration as a function of time is given by

$$\frac{\partial c}{\partial t} = D\nabla \cdot \left(\nabla c + \frac{c\nabla V}{kT}\right). \qquad [4]$$

The determination of this concentration $c(x, y, z, t)$ in the presence of a potential gradient requires solving this equation.

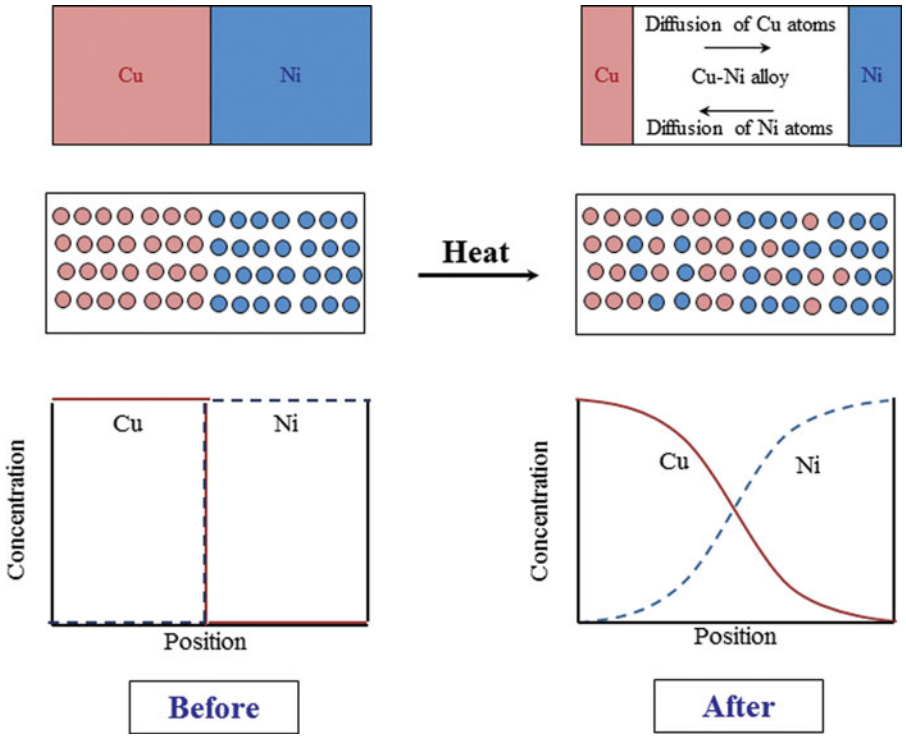

Fig. 3—Schematic example of self-diffusion process (color figure available online).

ACTIVATION ENERGY AND MODEL PARAMETERS

Buchwald and Heckel *(7)* were the first to utilize a diffusion-based model for the development of white etching bands in rolling contact fatigue. They suggested that the lenticular carbides that adjoin the white etching bands act as sinks for carbon solute because the carbon concentration just outside the lenticular carbides is nearly zero. Further, they proposed that the carbides dissolve in the white etching areas as a result of both the dilational compressive strains in these areas (due to localized plastic deformation) and the association of carbon with the increased dislocation density. However, the diffusion rates calculated using this model were many orders of magnitude smaller than that required for white etching bands and lenticular carbides' growth.

Part 1 (Warhadpande, et al. *(3)*) of this article describes that the formation of white bands is dependent on the bearing's operational load and, furthermore, there exists a threshold load level below which the development of white bands is not observed. In addition, several researchers proposed that there is a direct correlation between the formation of white etching bands and mild plastic deformation during rolling contact cycling. Thus, it can be interpreted that a driving force for carbon diffusion is due to the plastic deformation of the material and hence in this analysis the potential V employed in the stress-assisted diffusion (Eq. [4]) is set to be equal to the dissipated plastic energy. In other words, the gradient of dissipated plastic energy may drive the diffusion process for structural alterations in rolling contact fatigue. This is similar to the observations made by McGrath and Bratina *(20)*, who established that the phenomenon of fatigue in steel specimens resulted in the generation and movement of dislocations that intersect carbide particles and dissolve them. In these regions of localized deformation, pure ferrite zones free of carbide particles were formed. In an identical manner, a stress-assisted diffusion process may be the primary cause of band formation under rolling contact fatigue. Solid-state diffusion processes can be classified into two categories: (1) vacancy diffusion and (2) interstitial diffusion. Vacancy diffusion occurs when an atom jumps from an adjacent site into a surrounding vacancy in the crystal lattice, whereas interstitial diffusion occurs when an atom passes from one interstitial site to one of its neighboring interstitial sites without permanently displacing any of the matrix atoms. The structural changes during contact cycling are believed to occur due to interstitial diffusion of carbon atoms in the martensite matrix, as illustrated in Fig. 4. However, in order to jump from one interstitial site to another, the atoms need energy to break bonds with their neighbors and to cause the necessary lattice distortion during the jump process. This energy is called the *activation energy of diffusion*. Mitumura, et al. *(21)* conducted a study on

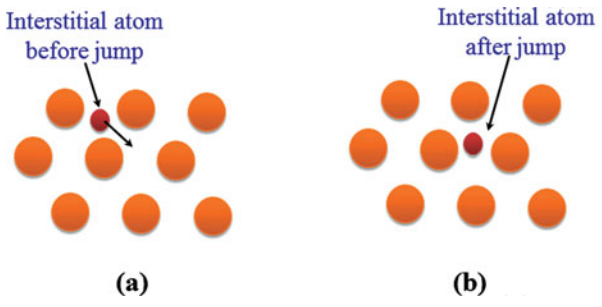

Fig. 4—Interstitial diffusion process (color figure available online).

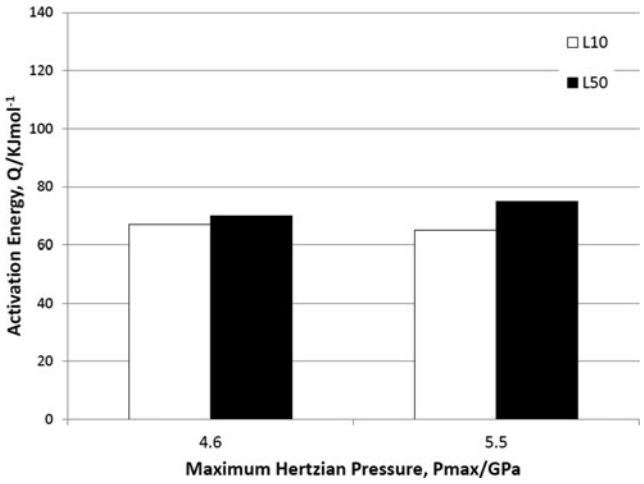

Fig. 5—Activation energy calculations as reported by Mitumura, et al. *(21)*.

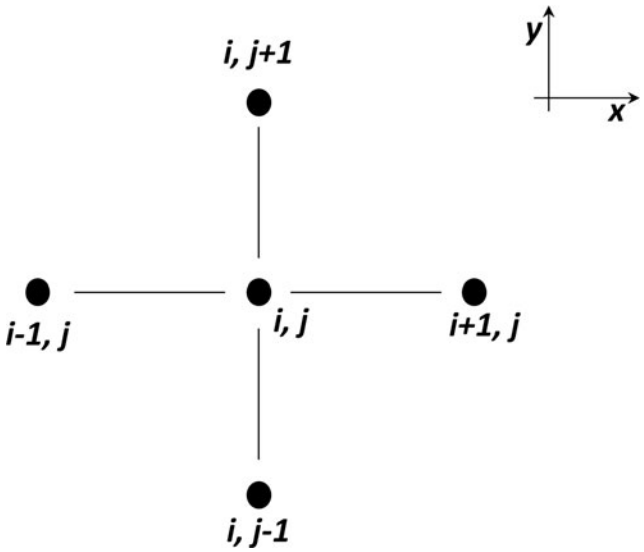

Fig. 6—Nodal definition for finite difference method.

activation energies during the diffusion processes that may occur during rolling contact fatigue. They reasoned that under certain circumstances, the rolling contact fatigue life of bearing steel is limited due to the structural changes occurring due to phase transformation. Because these phase changes are thought to be a kind of recrystallization (controlled by a diffusion process), the fatigue life can be expressed by an Arrhenius equation given as

$$L = Ae^{(-\frac{Q}{RT})}, \quad [5]$$

where L is the fatigue life, A is a constant, Q is the activation energy, and R is the gas constant, 8.314 J/(K.mol). In other words, the slope of the curve generated by plotting $\ln(L)$ versus $1/T$ provides the activation energy Q. Mitumura, et al. *(21)* conducted rolling contact fatigue studies at different temperatures and determined the activation energy. Figure 5 shows the activation energy arising during a fatigue process as obtained by Mitumura, et al. *(21)*. This activation energy is nearly the same despite two different loading conditions, which indicates that the rolling contact fatigue life limited by the formation of the phase changes is controlled by the same diffusion process. Furthermore, this activation energy closely matches the activation energy required for interstitial diffusion of carbon in ferrite, which is 84 kJ/mol. From this analysis, it is clear that carbon diffusion occurs during rolling contact fatigue, which leads to the decay of parent martensite structure, and the gradients of dissipated energy due to plastic deformation cause the development of white etching bands in the microstructure of bearing steels. In order to apply the diffusion equation, it is critical to identify the diffusion coefficient D used in Eq. [4]. The value of the diffusion coefficient is related to the activation energy in the following manner:

$$D = D_0 e^{(-\frac{Q}{RT})}, \quad [6]$$

where $D_0 = 2 \times 10^{-6}$ m^2/s for carbon in α-ferrite (Polansky and Keer *(22)*).

FINITE DIFFERENCE METHOD SOLUTION

In order to determine the localized carbon concentration changes during rolling contact fatigue processes, the stress-assisted diffusion Eq. [4] was solved using a finite difference scheme. An implicit backward Euler method was used to discretize the differential equation using the nodal definition as illustrated in Fig. 6. Equation [4] can be expanded as

$$\frac{\partial c}{\partial t} = D\nabla^2 c + \frac{D}{kT}\nabla c \cdot \nabla V + \frac{Dc}{kT}\nabla^2 V. \quad [7]$$

By employing the finite difference method, the discretized form of the above equation is given by

$$\begin{aligned}\frac{c_{i,j}^{n+1} - c_{i,j}^{n}}{\Delta t} = D\left[\frac{c_{i+1,j}^{n+1} - 2c_{i,j}^{n+1} + c_{i-1,j}^{n+1}}{\Delta h^2} + \frac{c_{i,j+1}^{n+1} - 2c_{i,j}^{n+1} + c_{i,j-1}^{n+1}}{\Delta h^2}\right] \\ + \frac{D}{kT}\left\{\left[\frac{c_{i+1,j}^{n+1} - c_{i,j}^{n+1}}{\Delta h}\right]\left[\frac{V_{i+1,j}^{n+1} - V_{i,j}^{n+1}}{\Delta h}\right]\right\} \\ + \frac{D}{kT}\left\{\left[\frac{c_{i,j+1}^{n+1} - c_{i,j}^{n+1}}{\Delta h}\right]\left[\frac{V_{i,j+1}^{n+1} - V_{i,j}^{n+1}}{\Delta h}\right]\right\} \\ + \frac{Dc_{i,j}^{n+1}}{kT}\left[\frac{V_{i+1,j}^{n+1} - 2V_{i,j}^{n+1} + V_{i-1,j}^{n+1}}{\Delta h^2}\right. \\ \left. + \frac{V_{i,j+1}^{n+1} - 2V_{i,j}^{n} + V_{i,j-1}^{n}}{\Delta h^2}\right]. \quad [8]\end{aligned}$$

The index n is for time step and i and j are for spatial coordinates. Δt and Δh correspond to temporal and spatial spans, respectively. Note that, during the diffusion process, there is no inflow or outflow of carbon atoms in the system in this analysis. Carbon is simply being redistributed in the material matrix where the white etching bands form. Thus, the total carbon concentration, before and after the diffusion process, must remain constant. Hence,

$$\begin{aligned}c_{i,j}^{n+1} + c_{i-1,j}^{n+1} + c_{i+1,j}^{n+1} + c_{i,j-1}^{n+1} + c_{i,j+1}^{n+1} = c_{i,j}^{n} + c_{i-1,j}^{n} + c_{i+1,j}^{n} \\ + c_{i,j-1}^{n} + c_{i,j+1}^{n}. \quad [9]\end{aligned}$$

Substituting Eq. [9] in Eq. [8] and solving for $c_{i,j}^{n+1}$ leads to

$$c_{i,j}^{n+1} = \frac{c_{i,j}^{n} + \frac{D\Delta t}{\Delta h^2}[c_{i,j}^{n} + c_{i-1,j}^{n} + c_{i+1,j}^{n} + c_{i,j-1}^{n} + c_{i,j+1}^{n}]}{1 + \frac{5D\Delta t}{\Delta h^2} - \frac{2D\Delta t}{kT\Delta h^2} V_{i,j}^{n+1} + \frac{D\Delta t}{kT\Delta h^2} V_{i+1,j}^{n+1} + \frac{D\Delta t}{kT\Delta h^2} V_{i,j+1}^{n+1} - \frac{D\Delta t}{kT}\nabla^2 V} + \frac{\frac{D\Delta t}{kT\Delta h^2}[c_{i+1,j}^{n+1} V_{i+1,j}^{n+1} - c_{i+1,j}^{n+1} V_{i,j}^{n+1} + c_{i,j+1}^{n+1} V_{i,j+1}^{n+1} - c_{i,j+1}^{n} V_{i,j}^{n+1}]}{1 + \frac{5D\Delta t}{\Delta h^2} - \frac{2D\Delta t}{kT\Delta h^2} V_{i,j}^{n+1} + \frac{D\Delta t}{kT\Delta h^2} V_{i+1,j}^{n+1} + \frac{D\Delta t}{kT\Delta h^2} V_{i,j+1}^{n+1} - \frac{D\Delta t}{kT}\nabla^2 V}. \quad [10]$$

The above equation provides the carbon concentration at any given point in time during the rolling contact simulation. Note that this study assumes that the potential gradients, which are the gradients of the dissipated plastic energy, do not change with time. Thus, all of the V^{n+1} can be replaced by V^n. Thus, from Eq. [10], the value of carbon concentration at $n + 1$ step is dependent on all the properties identified at n step except for two terms, namely, $c_{i+1,j}^{n+1}$ and $c_{i,j+1}^{n+1}$. Ideally, an iterative scheme should be employed to converge on the value for $c_{i,j}^{n+1}$. However, in order to obtain a solution in a reasonable amount of time, this analysis makes the following assumptions:

$$c_{i+1,j}^{n+1} = c_{i+1,j}^{n} \quad \text{and} \quad c_{i,j+1}^{n+1} = c_{i,j+1}^{n}. \quad [11]$$

Thus, Eq. [10] simplifies to

$$c_{i,j}^{n+1} = \frac{c_{i,j}^{n} + \frac{D\Delta t}{\Delta h^2}[c_{i,j}^{n} + c_{i-1,j}^{n} + c_{i+1,j}^{n} + c_{i,j-1}^{n} + c_{i,j+1}^{n}]}{1 + \frac{5D\Delta t}{\Delta h^2} - \frac{2D\Delta t}{kT\Delta h^2} V_{i,j}^{n} + \frac{D\Delta t}{kT\Delta h^2} V_{i+1,j}^{n} + \frac{D\Delta t}{kT\Delta h^2} V_{i,j+1}^{n} - \frac{D\Delta t}{kT}\nabla^2 V} + \frac{\frac{D\Delta t}{kT\Delta h^2}[c_{i+1,j}^{n} V_{i+1,j}^{n} - c_{i+1,j}^{n} V_{i,j}^{n} + c_{i,j+1}^{n} V_{i,j+1}^{n} - c_{i,j+1}^{n} V_{i,j}^{n}]}{1 + \frac{5D\Delta t}{\Delta h^2} - \frac{2D\Delta t}{kT\Delta h^2} V_{i,j}^{n} + \frac{D\Delta t}{kT\Delta h^2} V_{i+1,j}^{n} + \frac{D\Delta t}{kT\Delta h^2} V_{i,j+1}^{n} - \frac{D\Delta t}{kT}\nabla^2 V}. \quad [12]$$

MODEL APPLICATION

The most important term in the finite difference discretization presented in the previous section is the plastic dissipated energy V. In order to determine this dissipated energy, an elastic–plastic FE model previously developed by the authors was employed. Details on the elastic–plastic FE model for rolling contact fatigue can be found in Warhadpande, et al. *(18)*. The current model couples the elastic–plastic FE model with the finite difference scheme presented in the previous section in order to predict the formation of the white etching bands during rolling contact cycling. The following section presents the detailed solution strategy.

Solution Procedure

Part 1 of this article indicates that the orientation of the bands is dependent on the direction of load movement over the surface of the domain. If the load movement is from left to right, then the white etching bands are oriented from left to right sloping upwards and vice versa. In addition, the thickness of the 80° bands is quite large (up to 10 μm) compared to the size of the austenite grains. These facts suggest that the formation of the white etching bands may be independent of the bearing steel microstructure. Thus, a single FE mesh is sufficient to study the white band formation phenomenon. However, note that carbon migration occurs over very small distances, and hence the finite elements need to be very fine in order to capture the gradients accurately. For these purposes, the analysis domain was discretized using the Delaunay triangulation technique and, further, each triangular element was subdivided into three triangular elements, forming the constant strain FE mesh. Figure 7 illustrates the FE mesh used in this analysis. The length and depth of the domain are 10*b* and 7*b*, respectively, where *b* is the half contact width. (In this analysis. b = 100 μm.) This leads to 130,386 constant strain finite elements in the model. Note that the model is 2D and assumes plane strain conditions. One fatigue cycle consists of moving the Hertzian pressure over the domain from −3*b* to 3*b* in 41 steps. Figure 8 illustrates the elastic–plastic stress–strain curve modeled in this study. The hardening response is linear kinematic, which closely mimics the behavior of 52100 bearing steel (Bhargava, et al. *(23)*).

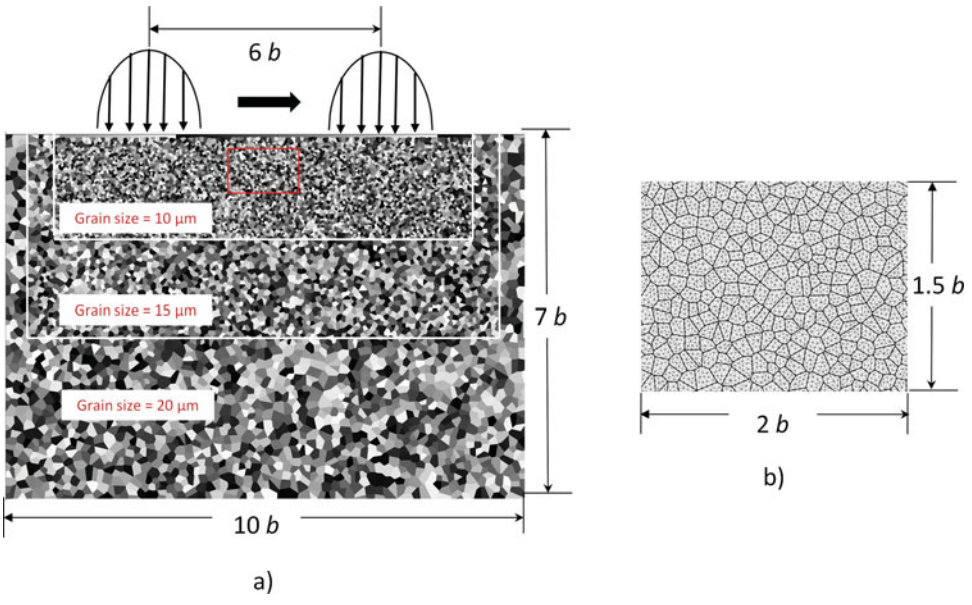

Fig. 7—(a) Finite element mesh used for diffusion model and (b) magnified view of the finite element mesh (color figure available online).

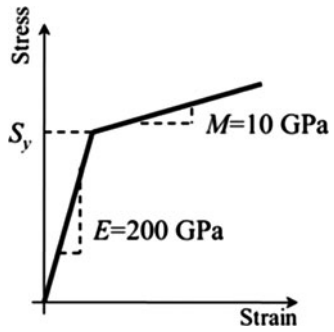

Fig. 8—Schematic linear hardening model.

Table 1 lists the material properties. At each location of load application, the Hertzian pressure is ramped up in 10 increments in order to perform the incremental plasticity calculations. Once the constitutive elastic–plastic equations are solved, the plastic strains and stresses experienced by each element in the domain are determined. Using this information, the dissipated energy due to plastic deformation is calculated as follows:

$$W_p = \left(\int_0^t \sigma_{ij}(\tau) \cdot \dot{\varepsilon}_{ij}^p(\tau)\, d\tau \right) A, \qquad [13]$$

where A is the area of the finite element. This dissipated energy W_p is the potential function V employed in the diffusion equation (Eq. [12]). After calculating V, the next step is to solve the diffusion equation. It was presented earlier that the diffusion equation is solved using a finite difference scheme. In order to perform the finite difference calculation, the spatial data for the dissipated plastic energy (V) first calculated at each node of the FE mesh is transferred onto a uniform mesh/square grid, and using the information at each node of this uniform grid, Eq. [12] is solved and new carbon concentrations are determined. The uniform grid is constructed by spacing the nodes at equal $\Delta h = 1/3$ μm intervals in the X and Y directions. The value of dissipated plastic energy/carbon concentration at each node of the uniform grid is determined by the value of that particular quantity at the nearest location of the node of the FE mesh. This gives an approximate solution for the dissipated plastic energy/carbon concentration for the nodes of the finite difference grid; however, because the FE mesh is extremely fine, no significant loss of information occurs by employing this procedure with the advantage of improved computation time. Note that this approach neglects the dependence of the diffusion coefficient on stress. The diffusion coefficient may be affected by the stress histories experienced by the material; however, such dependence is beyond the scope of the current analysis. Similarly, the diffusion coefficient is affected by the temperature history (see Eq. [6]). However, in the range of temperature observed by the bearing steel during normal operation, using Eq. [6], it can be observed that the diffusion coefficient remains fairly constant. Thus, it is assumed that the diffusion coefficient remains constant throughout the simulation. Once the new carbon concentrations are determined, the load is moved to a new location on the FE domain and the procedure is repeated. Ideally, the material properties (E, ν, M, σ_y) for the material elements will change with the change in carbon concentration. However, there are no data available in the literature showing the dependence of the material properties on carbon concentration for bearing steel. Furthermore, the stress-assisted diffusion equation assumes continuum behavior for the subsurface microstructure, with no account for heterogeneity influences on diffusion or reaction–diffusion behavior as carbon migrates through the structure. Hence, the current FE model assumes no coupling between the carbon concentrations and the constitutive material behavior. Once the plastic strains and stresses for each 41 steps of load application are determined, there is no need to recalculate them for the next cycle. By simply evaluating the differential equation, the change in carbon concentrations can be determined for the following cycles.

TABLE 1—MATERIAL PROPERTIES

Elastic modulus (E)	200 GPa
Hardening modulus (M)	10 GPa
Yield limit (Sy)	2,030 MPa
Poisson's ratio (ν)	0.3

Data from Warhadpande, et al. *(18)*.

Δt Calculations and Jump-In Cycle Procedure

As described in the previous section, Eq. [12] is used to solve the diffusion equation and determine the change in carbon concentration from the Hertzian pressure. The time span for the diffusion process represented by each loading application is defined by the parameter Δt in Eq. [12]. In this model, Δt is the time required for the load to move from one location to another. As indicated earlier, one load pass includes a move of the Hertzian pressure over the surface of the domain from $-3b$ to $3b$ in 41 steps. The half contact width $b = 100$ μm and, hence, in each step the load is moved by

$$\Delta x = \frac{600\mu m}{40} = 15\mu m. \qquad [14]$$

The time required for the roller to travel Δx depends on the speed of the bearing and bearing geometry. Assuming a speed of 3,600 rpm,

$$\Delta t = \frac{60}{3600 * 2\pi r} * 15 \times 10^{-6}\text{s} = \frac{125 \times 10^{-9}}{\pi r}\text{s}. \qquad [15]$$

Thus, it can be deduced that the order of magnitude for Δt ranges from approximately 10^{-8} to 10^{-10} s. In this model, the value for Δt was set to 10^{-10} s.

White etching bands in bearing steel microstructure generally are not observed to develop until about 10^7 to 10^8 cycles. Over these large numbers of cycles, the localized drop in carbon concentration is only about 0.8 wt% (going from 1 wt% for a pristine microstructure to 0.2 wt% for 30° bands). Thus, the relative change in carbon concentration over one cycle is negligible. This agrees with Swahn, et al.'s *(24)* observations. Hence, it is computationally very expensive to solve the diffusion equation for every rolling contact cycle. Instead, a jump-in-cycle procedure is adopted here in order to arrive at the solution in reasonable amount of computational cycles. The jump-in-cycle procedure is summarized below:

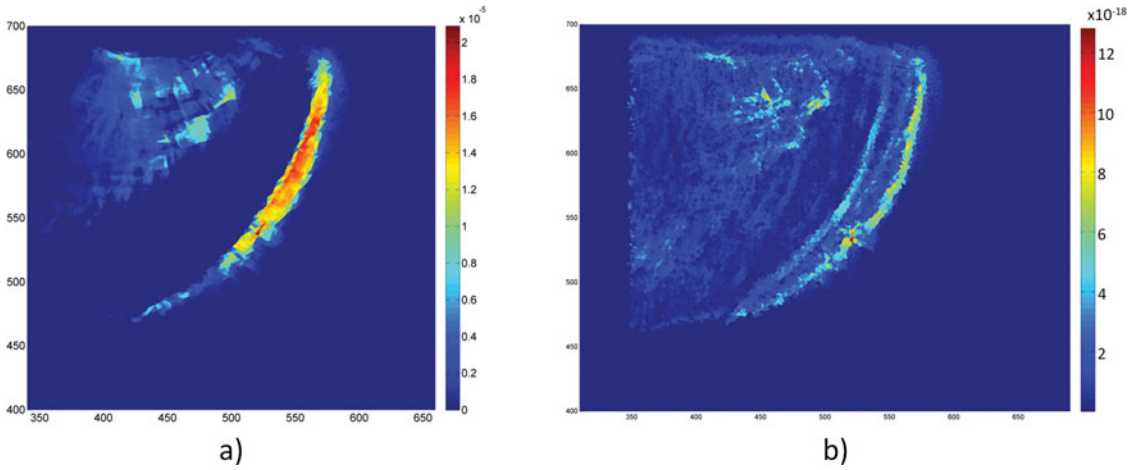

Fig. 9—Contour plot showing the magnitude of (a) dissipated plastic energy per unit volume and (b) stress-assisted diffusion flux during a typical loading cycle (color figure available online).

1. Before the start of the simulation, the carbon concentration is assumed to be homogenously distributed in each finite element,

$$c_j^0 = 1\text{wt}\%. \quad [16]$$

2. The Hertzian pressure is moved over the domain and dissipated energy due to plastic deformation is determined. Using this dissipated energy and diffusion equation, the carbon concentrations are determined at each step of load application.
3. By comparing the values of carbon concentrations before and after the cycle, the change in carbon concentration over one cycle, $(\frac{dc}{dN})_j^i$, is determined.
4. Using the values of $(\frac{dc}{dN})_j^i$ for all of the finite elements, the maximum rate of change of carbon concentration is determined. Next, it is assumed that over a block of ΔN cycles, carbon concentration for the element with the maximum change in carbon concentration will change by a certain fixed amount Δc. The value of Δc is a compromise between solution accuracy and computation expense. After conducting extensive sensitivity analysis (not shown here), a value of $\Delta c = 0.02$ was chosen that provides satisfactory results in a reasonable time.
5. Thus, the number of cycles for the current block of cycles becomes

$$\Delta N^i = \frac{\Delta c}{\left(\frac{dc}{dN}\right)_{max}^i}. \quad [17]$$

6. The cycle numbers are updated as

$$N = N + \Delta N^i. \quad [18]$$

7. Next, the carbon concentration at the end of this block of cycles is updated as follows:

$$c_j^{i+1} = c_j^i + \left(\frac{dc}{dN}\right)_j^i \Delta N^i. \quad [19]$$

Once the carbon concentration is updated at the end of each block of ΔN cycles, the algorithm is repeated from step 2 through step 7. The next section describes the implementation of the above-mentioned algorithm for predicting the formation of white etching bands during rolling contact fatigue.

Stress-Assisted Diffusion Flux

As described in the section on Fick's law of diffusion, a stress-assisted diffusion law is employed in order to predict the formation of the white etching bands under rolling contact fatigue. Using the algorithm presented in the previous section, the differential equation was solved and the magnitude and directions of the diffusion flux were determined as given by Eq. [3]. Table 2 shows the model parameters used for the current sample analysis. Figures 9 and 10 illustrate the results obtained for this case. Figure 9a shows the dissipated plastic energy per unit volume, whereas Fig. 9b depicts the magnitude of diffusion flux when the load is positioned at the center of the domain. Furthermore, Fig. 10 illustrates the direction of the diffusion flux. From Fig. 9b it is clear that the diffusion flux is at its maximum in the areas highlighted in the red boxes. A closer examination of the direction of the diffusion flux, as illustrated in Fig. 10, reveals that the directions are inclined at certain angles to the surface of the domain. The diffusion flux in the deeper region in Fig. 10 is inclined at an angle of about 25–40° to the surface, whereas the one in the shallower region is inclined at an angle of about 75–80°. These angles correspond to the orientations of the white etching bands commonly observed in fatigued bearing microstructure. In addition, the depths are consistent with the experimental observations. The diffusional flux oriented at about 25 to 40° is about 1*b* to 1.5*b* deep in the domain, whereas the diffusional flux oriented at about 75 to 80° lies from 0.5*b* to 1*b* deep

TABLE 2—MODEL PARAMETERS

Model Parameter	Parameter Value
P_h	4.5 GPa
μ	0.05
D	3.44×10^{-18} m^2/s
T	373 K

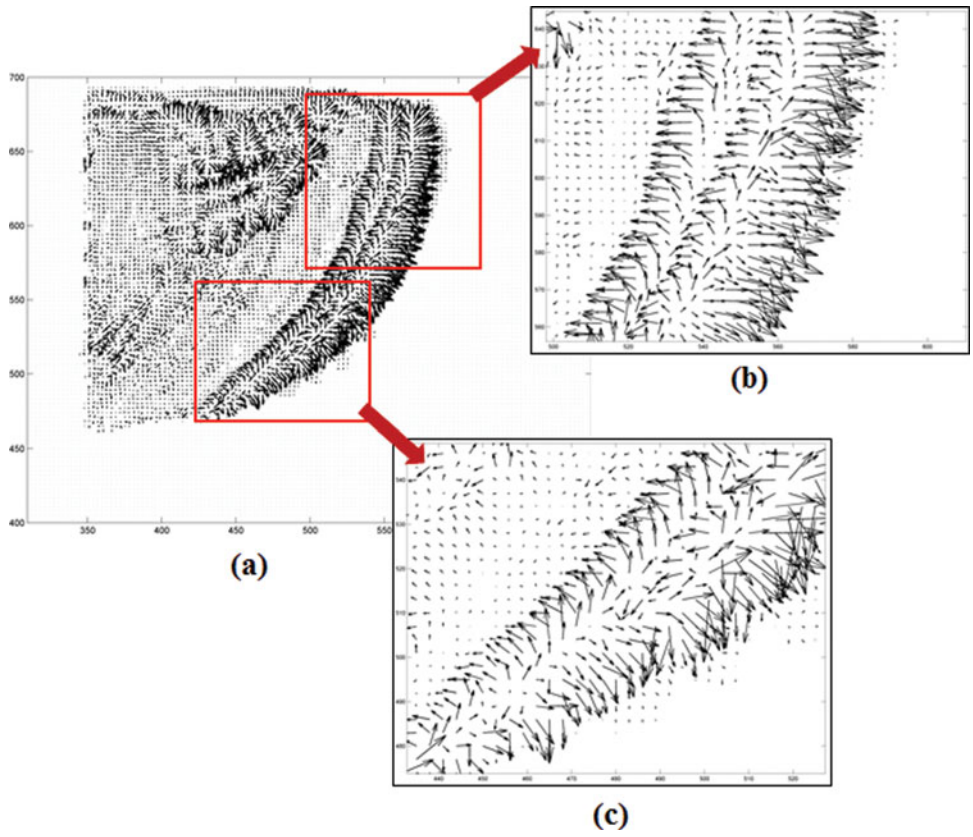

Fig. 10—(a) Vector plot illustrating the direction of the stress-assisted diffusion flux, (b) gradients closer to the surface lead to the formation of high angle bands, and (c) gradient deeper in the domain lead to the formation of low angle bands (color figure available online).

in the domain. These depths closely match the depths for the 30 and 80° white etching bands. Thus, it is proposed that carbon diffusion will occur along these orientations at each step of load application. The carbon diffusion gives rise to areas of low carbon concentration, permitting the formation of white etching regions. In addition, the carbon that diffuses out of the bands accumulates in the adjoining areas and is precipitated as lenticular carbides.

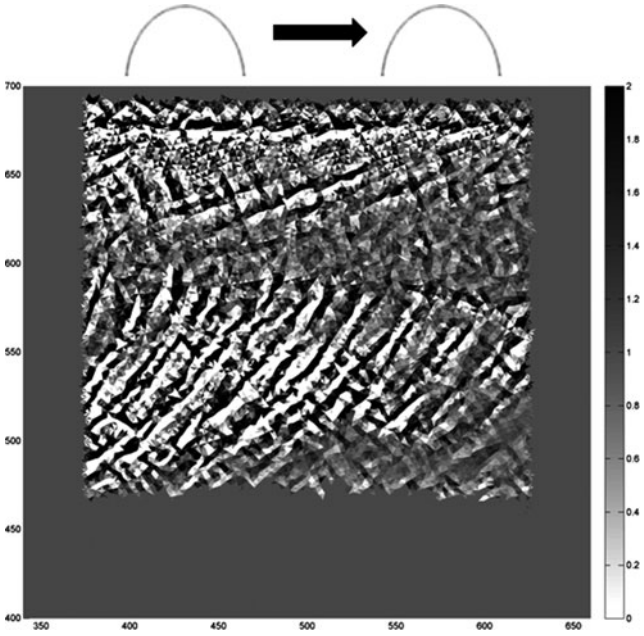

Fig. 11—Carbon concentration plot for load movement from left to right.

Numerical Prediction of Band Formation

This section presents the band formation process for two sample cases. Figure 11 depicts the carbon concentration plot in the domain after $N = 1 \times 10^7$ cycles. Note that the direction of load movement for this case is left to right. The color map selected is such that lighter grey areas correspond to low carbon concentration and darker region portray regions of high carbon concentration. The white regions develop in the form of equally spaced bands in the material domain separated by regions of darker regions. The white regions have lower carbon concentration and hence are the white etching bands, whereas the darker regions are areas of high carbon concentration and hence they are the lenticular carbides found adjacent to the white bands in fatigued bearings. The angles of the white bands range from 25 to 40°, matching the experimentally observed orientation of white etching bands. In addition, their depths range from 1*b* to 1.5*b*, which is consistent with experimental observation. Figure 12 depicts the carbon concentration plots for the case of moving the Hertzian pressure from right to left. The results indicate that with the change in the load movement direction, the bands reverse their orientation, consistent with the experimental findings (as described in Part 1 of this article). Thus, the stress-assisted diffusion-based model is able to predict the formation of 30° white etching bands with

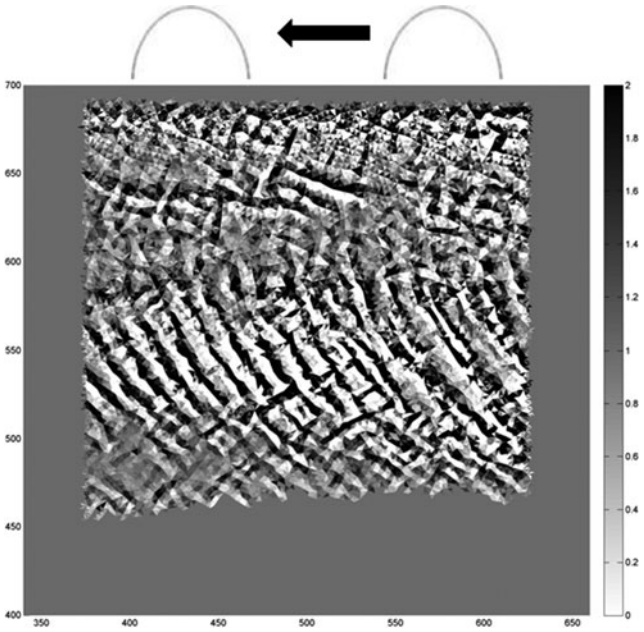

Fig. 12—Carbon concentration plot for load movement from right to left.

good experimental corroboration. The analysis of diffusion flux in the previous section indicated that toward the surface of the domain, the flux is oriented at an angle of about 75 to 80°. However, similar observations cannot be made for the white bands near the surface. It is difficult to separate the bands closer to the surface. The primary reason for this is that in the current model, there is no coupling between the carbon concentrations and the material properties of the finite elements. As pointed out in Part 1 (Warhadpande, et al. *(3)*) of this article, the formation of 80° bands is due to the stress concentration that arises due to the development of 30° bands. Due to the lack of coupling between material properties and carbon concentration, the current model does not capture the stress concentrations arising due to carbon diffusion. Hence, the formation of 80° bands is not as prominent as the formation of 30° bands using the current analysis approach.

The two cases presented above are for the Hertzian pressure of 4.5 GPa, which is admittedly high compared to typical bearing application conditions. The analysis was repeated for different loads ranging from 3.5 to 5.5 GPa and the results were evaluated. Table 3 depicts the metallurgical properties of the different phases that evolve during rolling contact cycling. From the table it can be estimated that 30° bands have a carbon concentration of about 0.2 wt%. Thus, as an approximation, the number of cycles required for a band to reach a carbon concentration of 0.2 wt% will be the minimum number of cycles required for the formation of 30° bands. Another important parameter to consider while determining the cycles for 30° band formation is the value for Δt, as described in the subsection on Δt calculations. The value of Δt, which is dependent on the bearing geometry and operating speed, plays a significant role in deciding the cycle number. The current analysis employed three different values of Δt, namely, 10^{-8}, 10^{-10}, and 10^{-12}, and determined the number of cycles required for the development of 30° bands. These cycle numbers were evaluated for different Hertzian pressures ranging from 3.5 to 5.5 GPa and plotted on a P-N (load-cycle) diagram in order to compare with the experimentally observed values as illustrated in Fig. 13. The cycle numbers obtained using the current model using all three values of Δt are within reasonable agreement with experimental observations. It is important to note that the experimental data set presented in Fig. 13 is a compendium of disparate sources and is a mix of both line and

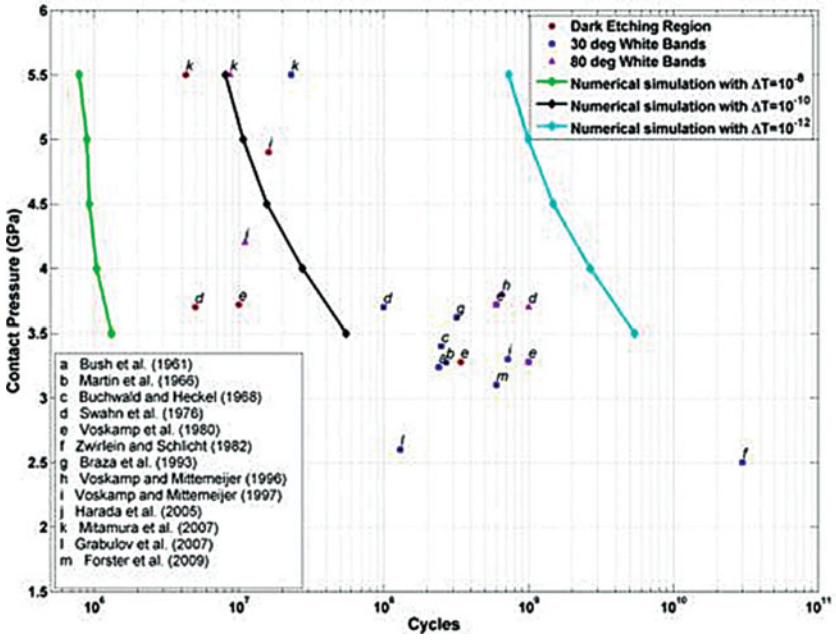

Fig. 13—Comparison of experimentally and numerically obtained number of cycles for structural alterations (color figure available online).

TABLE 3—METALLURGICAL PROPERTIES OF THE ALTERED MICROSTRUCTURE AFTER CONTACT YIELDING

Region	Metallurgical Composition	% C	% Fe	% Cr	% Mn
Dark etching region	Ferrite + retained martensite	Nearly the same as the base microstructure	96.5–97.0	1.9–2.1	0.4–0.5
30° Bands	Ferrite with some carbide	~0.2	96.3–96.5	1.9–2.3	0.6–0.8
80° Bands	Purely ferrite	~0.0	96.3–96.5	1.9–2.3	0.6–0.8

Data from Beswick *(25)* and Muroga and Saka *(26)*.

point contact analysis. Additionally, the material used in the literature analyses might vary based on the manufacturing processes employed. Hence, the comparison is more qualitative than quantitative and is performed in order to display the capability of the current model methodology to predict the cycle number required for the formation of white etching band.

SUMMARY AND CONCLUSIONS

Microstructural changes that occur in bearing steel during rolling contact cycling have been a topic of significant research and discussion since 1947. These structural changes are more popularly known as the dark and white etching phenomena. One of the most puzzling aspects of these microstructural changes is the repeatable orientation of the white etching bands. Researchers in the past have evaluated different theories in order to explain their orientation. However, none of these theories satisfactorily explains the inclination of the white etching bands. The accepted cause of these structural alterations is decay of martensite due to interstitial carbon diffusion. To this end, the elastic–plastic FE model developed in a previous study (Warhadpande, et al. *(18)*) was coupled with a stress-assisted diffusion model in this work to predict the migration directions of carbon during rolling contact cycling. Because material plasticity is known to be directly related to the formation of white etching bands, the potential driving the diffusion process was assumed to be the energy dissipated due to plastic deformation. Using an implicit backward Euler finite difference routine, Fick's law for stress-assisted diffusion was discretized and the carbon concentrations due to the application of Hertzian pressure were determined. The results indicated that the carbon migration occurred along specific orientations due to gradients in the dissipated plastic energy. The regions of depleted carbon concentration may constitute the white etching bands and are oriented at 25 to 40° deeper in the domain (1*b* to 1.5*b*) and at 70 to 80° closer to the surface (0.5*b* to 1*b*). These results are in good agreement with the experimental observation. In addition, it is demonstrated that if the speed and geometry of the bearing are known, the model can predict the number of cycles required for the development of the white etching bands with reasonable accuracy.

REFERENCES

(1) Jones, A. B. (1947), *Metallographic Observations of Ball Bearing Fatigue Phenomenon*, ASTM: Philadelphia.

(2) Lund, T. (1969), "Structural Alterations in Fatigue-Tested Ball-Bearing Steel," *Jernkontorets Annaler*, **153**(7), pp 337–343.

(3) Warhadpande, A., Sadeghi, F., & Evans, R. D. (2013), "Microstructural Alterations in Bearing Steels under Rolling Contact Fatigue Part 1—Historical Overview," *Tribology Transactions*, **56**(3), pp 349–358.

(4) Bhadeshia, H. K. D. H. (2012), "Steels for Bearings," *Progress in Materials Science*, **57**(2), pp 268–435.

(5) Bush, J. J., Grube, W. L., and Robinson, G. H. (1961), "Microstructural and Residual Stress Changes in Hardened Steel Due to Rolling Contact," *Transactions of the ASM*, **54**, pp 390–412.

(6) Martin, J. A., Borgese, S. F., and Eberhard, A. (1966), "Microstructural Alterations of Rolling–Bearing Steel Undergoing Cyclic Stressing," *Journal of Basic Engineering*, **88**, No. 3, pp 555–565.

(7) Buchwald, J. and Heckel, R. W. (1968), "An Analysis of Microstructural Changes in 52100 Steel Bearings during Cyclic Stressing," *Transactions of the ASM*, **61**(4), pp 750–756.

(8) Osterlund, R. and Vingsbo, O. (1980), "Phase-Changes in Fatigued Ball-Bearings," *Metallurgical Transactions A - Physical Metallurgy and Materials Science*, **11**(5), pp 701–707.

(9) Lindahl, E. and Osterlund, R. (1982), "$2\frac{1}{2}$D Transmission Electron-Microscopy Applied to Phase-Transformations in Ball-Bearings," *Ultramicroscopy*, **9**(4), pp 355–364.

(10) Avarami, M. (1940), "Kinetics of Phase Change Part II: Transformation Time Relations for Random Distribution of Nuclei," *Journal of Chemical Physics*, **8**, pp 212–224.

(11) Avrami, M. (1939), "Kinetics of Phase Change Part I: General Theory," *Journal of Chemical Physics*, **7**, pp 1103–1112.

(12) Avrami, M. (1941), "Kinetics of Phase Change Part III: Granulation, Phase Change, and Microstructure," *Journal of Chemical Physics*, **9**, pp 177–184.

(13) Christian, J. W. (2002), *The Theory of Transformation in Metals and Alloys*, Pergamon: London.

(14) Suehiro, M., Senuma, T., Yada, H., and Sato, K. (1992), "Application of Mathematical Model for Predicting Microstructural Evolution to High Carbon Steels," *ISIJ International*, **32**, pp 433–439.

(15) Ronda, J. and Oliver, G. J. (2000), "Consistent Thermo-Mechano-Metallurgical Model of Welded Steel with Unified Approach to Derivation of Phase Evolution Laws and Transformation-Induced Plasticity," *Computer Methods in Applied Mechanics and Engineering*, **189**(2), pp 361–417.

(16) Pernach, M. and Pietrzyk, M. (2008), "Numerical Solution of the Diffusion Equation with Moving Boundary Applied to Modeling of the Austenite–Ferrite Phase Transformation," *Computational Materials Science*, **44**, pp 783–791.

(17) Zhou, L. G. (2011), "Modeling of Oxygen Diffusion along Grain Boundaries in a Nickel-Based Superalloy," *Journal of Engineering Materials and Technology*, **133**, pp 031002-1–031002-7.

(18) Warhadpande, A., Sadeghi, F., Kotzalas, M. N., and Doll, G. (2012), "Effects of Plasticity on Subsurface Initiated Spalling in Rolling Contact Fatigue," *International Journal of Fatigue*, **36**(1), pp 80–95.

(19) Shewmon, P. G. (1963), *Diffusion in Solids*, McGraw Hill, New York.

(20) McGrath, J. T. and Bratina, W. J. (1967), "Interaction of Dislocations and Precipitations in Quench-Aged Iron–Carbon Alloys Subjected to Cyclic Stressing," *Acta Metallurgica*, **2**, pp 239–339.

(21) Mitamura, N., Hidaka, H., and Takaki, S. (2007), "Microstructural Development in Bearing Steel during Rolling Contact Fatigue," *Materials Science Forum*, **539–643**, pp 4255–4260.

(22) Polonsky, I. A. and Keer, L. M. (1995), "Om White Etching Band Formation in Rolling Bearings," *Journal of the Mechanics and Physics of Solids*, **43**(4), pp 637–669.

(23) Bhargava, V., Hahn, G. T., and Rubin, C. A. (1985), "An Elastic–Plastic Finite Element Model of Rolling Contact, Part 1: Analysis of Single Contacts," *ASME Journal of Applied Mechanics*, **52**, pp 67–74.

(24) Swahn, H., Becker, P. C., and Vingsbo, O. (1976), "Electron-Microscope Studies of Carbide Decay during Contact Fatigue in Ball Bearings," *Metal Science*, **10**, pp 35–39.

(25) Beswick, J. M. (1975), "Measurement of Carbon Levels in Structurally Transformed SAE 52100 Ball Bearing Steel by Microprobe Analysis," *Practical Metallography*, **12**, pp 200–206.

(26) Muroga, A. and Saka, H. (1995), "Analysis of Rolling Contact Fayigue Microstructure Using Focused Ion-Beam Sputtering and Transmission Electron-Microscopy," *Scripta Metallurgica et Materialia*, **33**(1), pp 151–156.